The Astrophysical Journal, 595:555–563, 2003 September 20

PARTICLE ACCELERATION IN RELATIVISTIC JETS DUE TO WEIBEL INSTABILITY

K.-I. Nishikawa[1]
National Space Science and Technology Center, Huntsville, AL 35805; ken-ichi.nishikawa@nsstc.nasa.gov

P. Hardee
Department of Physics and Astronomy, University of Alabama, Tuscaloosa, AL 35487

G. Richardson[1]
National Space Science and Technology Center, Huntsville, AL 35805

R. Preece
Department of Physics, University of Alabama, Huntsville, AL 35899; and National Space Science and Technology Center, Huntsville, AL 35805

H. Sol
LUTH, Observatore de Paris-Meudon, 5 place Jules Jansen, 92195 Meudon Cedex, France

and

G. J. Fishman
NASA Marshall Space Flight Center, National Space Science and Technology Center, 320 Sparkman Drive, SD 50, Huntsville, AL 35805
Received 2003 May 6; accepted 2003 May 28

ABSTRACT

Shock acceleration is a ubiquitous phenomenon in astrophysical plasmas. Plasma waves and their associated instabilities (e.g., the Buneman instability, two-streaming instability, and the Weibel instability) created in the shocks are responsible for particle (electron, positron, and ion) acceleration. Using a three-dimensional relativistic electromagnetic particle code, we have investigated particle acceleration associated with a relativistic jet front propagating through an ambient plasma with and without initial magnetic fields. We find only small differences in the results between no ambient and weak ambient magnetic fields. Simulations show that the Weibel instability created in the collisionless shock front accelerates particles perpendicular and parallel to the jet propagation direction. While some Fermi acceleration may occur at the jet front, the majority of electron acceleration takes place behind the jet front and cannot be characterized as Fermi acceleration. The simulation results show that this instability is responsible for generating and amplifying highly nonuniform, small-scale magnetic fields, which contribute to the electron's transverse deflection behind the jet head. The "jitter" radiation from deflected electrons has different properties than synchrotron radiation which is calculated in a uniform magnetic field. This jitter radiation may be important to understanding the complex time evolution and/or spectral structure in gamma-ray bursts, relativistic jets, and supernova remnants.

Subject headings: acceleration of particles — instabilities — shock waves
On-line material: color figures

1. INTRODUCTION

Nonthermal radiation, usually having a power-law emission spectrum, has been observed from astrophysical systems containing relativistic jets, e.g., active galactic nuclei (AGNs), gamma-ray bursts (GRBs), Galactic microquasar systems, and Crab-like supernova remnants. In most of these systems, the emission is thought to be generated by accelerated electrons via the synchrotron or inverse Compton mechanisms. Radiation is observed from these systems from the radio through the gamma-ray regions.

The most widely known mechanism for the acceleration of particles in astrophysical environments characterized by a power-law spectrum is Fermi acceleration. This mechanism for particle acceleration relies on the shock jump conditions at relativistic shocks (e.g., Gallant 2002). Most astrophysical shocks are collisionless since dissipation is dominated by wave-particle interactions rather than by particle-particle collisions. Diffusive shock acceleration (DSA) relies on repeated scattering of charged particles by magnetic irregularities (Alfvén waves) to confine the particles near the shocks. However, particle acceleration near relativistic shocks is not due to DSA because the propagation of accelerated particles ahead of the shock cannot be described as spatial diffusion. Anisotropies in the angular distribution of the accelerated particles are large, and the diffusion approximation for spatial transport does not apply (Achterberg et al. 2001). Particle-in-cell (PIC) simulations may shed light on the physical mechanism of particle acceleration that involves the complicated dynamics of particles in relativistic shocks.

Recent PIC simulations using counterstreaming relativistic jets show that acceleration is provided in situ in the downstream jet, rather than by the scattering of particles back and forth across the shock as in Fermi acceleration (Frederiksen et al. 2003). Two independent simulation studies have confirmed that the counterstreaming jets excite the Weibel instability (Weibel 1959), which generates magnetic fields (Medvedev & Loeb 1999; Brainerd 2000; Pruet, Abazajian, & Fuller 2001; Gruzinov 2001) and consequently

[1] NRC Associate, NASA Marshall Space Flight Center.

accelerates electrons (Silva et al. 2003; Frederiksen et al. 2003). Since these simulations are performed with counterstreaming jets, shock dynamics involving the jet head, where Fermi acceleration may take place, has not been investigated.

In this paper we present new simulation results of particle acceleration and magnetic field generation in relativistic jets using three-dimensional relativistic electromagnetic particle-in-cell (REMP) simulations with and without initial ambient magnetic fields. In our simulations, an electron-ion relativistic jet with Lorentz factor, $\gamma = 5$ (corresponds to 5 MeV), is injected into an electron-ion plasma in order to study the dynamics of a relativistic collisionless shock. We illustrate the features of the collisionless shock generated at the head of the relativistic jet injected into magnetized and unmagnetized ambient plasma. The Weibel instability is excited in the downstream region and accelerates electrons and ions. In § 2 the simulation model and initial conditions are described. The simulation results are presented in § 3, and in § 4 we summarize and discuss the results.

2. SIMULATION MODEL

The code used in this study is a modified version of the TRISTAN code, which is a relativistic electromagnetic particle (REMP) code (Buneman 1993). Descriptions of PIC codes are presented in Dawson (1983), Birdsall & Langdon (1995), and Hockney & Eastwood (1988). This code has been used for many applications including astrophysical plasmas (Zhao et al. 1994; Nishikawa et al. 1997).

The simulations were performed using $85 \times 85 \times 160$ grids with a total of 55–85 million particles (27 particles per cell per species for the ambient plasma). Both periodic and radiating boundary conditions are used (Buneman 1993). The ambient electron and ion plasma has mass ratio $m_i/m_e = 20$. The electron thermal velocity v_e is $0.1c$, where c is the speed of light. The electron skin depth, $\lambda_{ce} = c/\omega_{pe}$, is 4.8Δ, where $\omega_{pe} = (4\pi e^2 n_e/m_e)^{1/2}$ is the electron plasma frequency (Δ is the grid size). In this study, three different cases are simulated to investigate the fundamental characteristics of the Weibel instability in electron-ion plasmas. One simulation is performed by injecting a thin jet into a magnetized ambient plasma. The other two simulations consider flat jets (infinite width) injected into a magnetized ambient plasma and then into an unmagnetized ambient plasma in order to compare this simulation with previous simulations (Silva et al. 2003; Frederiksen et al. 2003).

3. SIMULATION RESULTS

3.1. *Injection into Magnetized Ambient Plasma*

3.1.1. *Thin Jet*

Two kinds of jets have been simulated: a "thin" jet with radius $r_{\rm jet} = 4\Delta$ and a "flat" (thick) jet that fills the computational domain in the transverse directions (infinite width). In the simulations, jets are injected at $z = 25\Delta$. First, we describe the simulation results for the thin jet with initial ambient magnetic fields. The number density of the thin jet is $0.741n_b$, where n_b is the density of ambient (background) electrons. The average jet velocity $v_j = 0.9798c$, and the Lorentz factor is 5. The time step $\omega_{pe}\Delta t = 0.026$, the ratio $\omega_{pe}/\Omega_e = 2.89$, the Alfvén speed $v_{\rm A} = 0.0775c$, and the Alfvén Mach number $M_{\rm A} = v_j/v_{\rm A} = 12.65$. The gyroradii of ambient electrons and ions are 1.389Δ and 6.211Δ, respectively. As shown in Figure 1, the jet electrons are twisted due to a two-stream–type instability. Since the size of jet is of the order of the electron skin depth, it is not clear if the Weibel instability is excited. As will be shown in the flat jet simulation, the density perturbation is similar to that induced by the Weibel instability. Since the size of the jet is extremely small compared to realistic jets, further study of thin jets will be performed including simulations with larger jet sizes.

3.1.2. *Flat Jet*

The jet density of the flat jet is also nearly $0.741n_b$. Other parameters are the same as in the case of the thin jet. In this

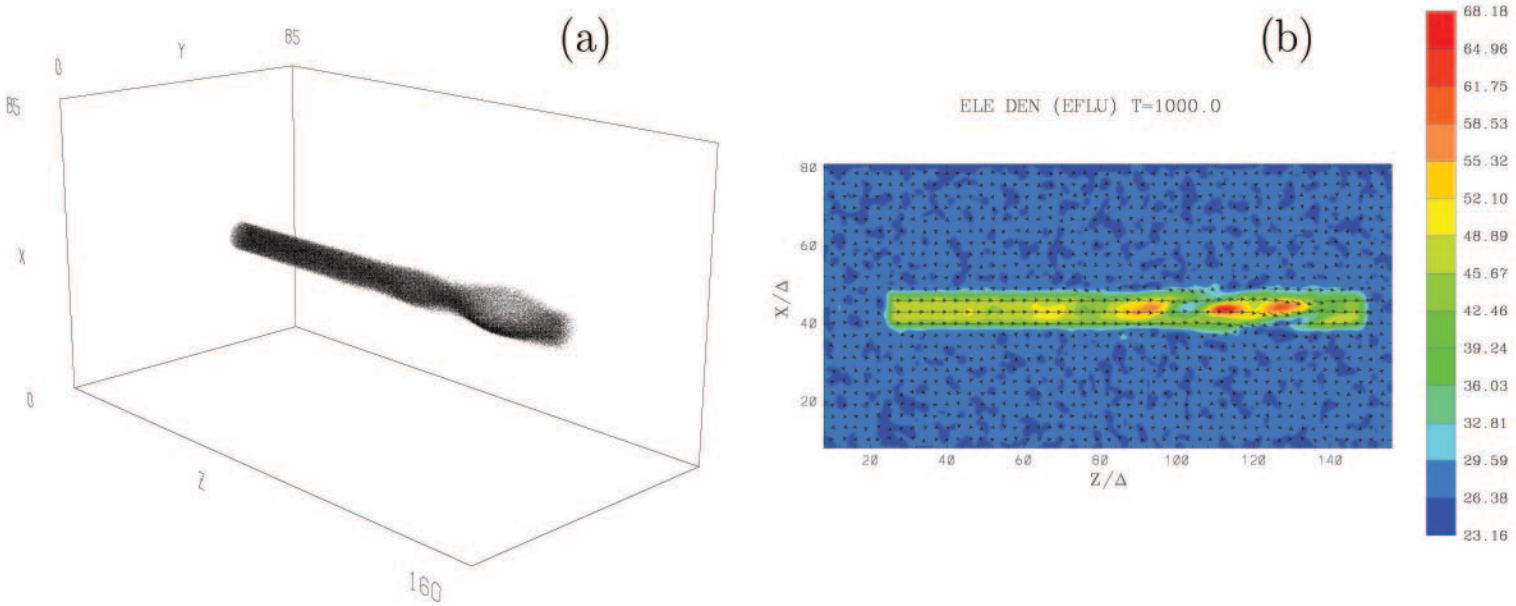

FIG. 1.—Dynamics of the thin jet are indicated at $\omega_{pe}t = 26$ by (*a*) a jet electron image in the three-dimensional simulation system and (*b*) the total electron density in the *x*-*z* plane in the center of the jet with the electron flux indicated by arrows and density indicated by color. A two-stream–type instability twists the jet electrons as shown in these plates. [*See the electronic edition of the Journal for a color version of this figure.*]

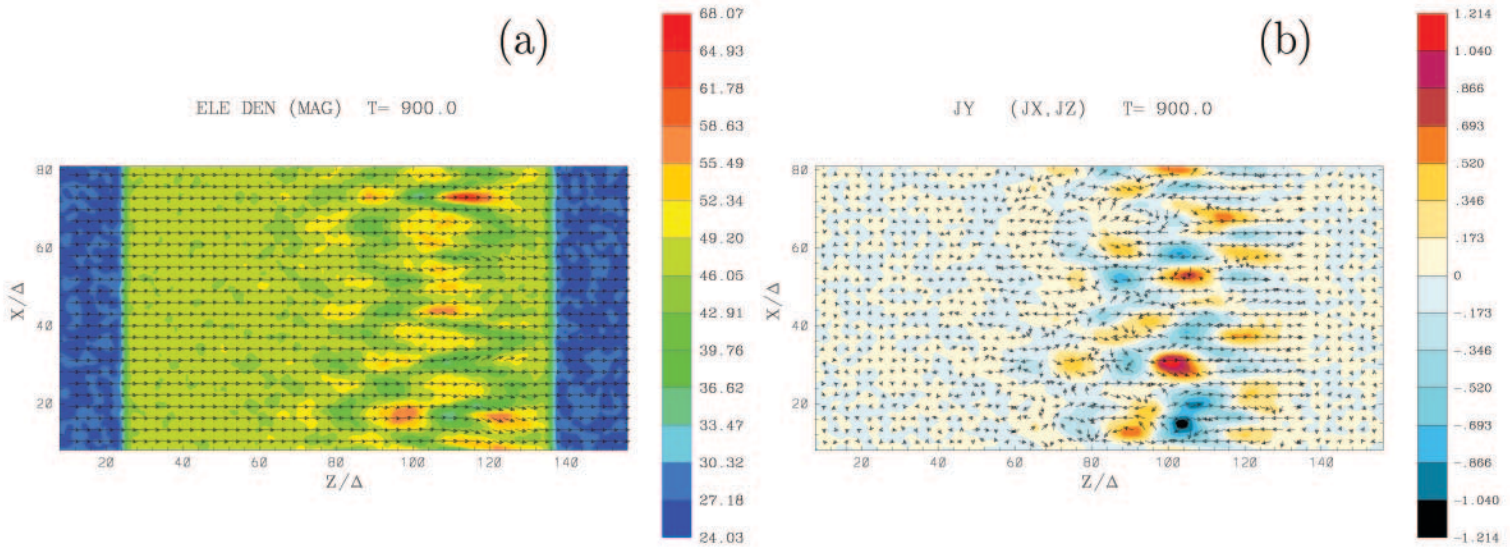

FIG. 2.—Weibel instability for the flat jet is illustrated in two-dimensional images in the x-z plane ($y = 43\Delta$) in the center of the jet at $\omega_{pe}t = 23.4$. In (*a*) the colors indicate the electron density with magnetic fields represented by arrows; in (*b*) the colors indicate the y-component of the current density (J_y) with J_z, J_x indicated by the arrows. The Weibel instability perturbs the electron density, leading to nonuniform currents and highly structured magnetic fields. [*See the electronic edition of the Journal for a color version of this figure.*]

case, the jet makes contact with the ambient plasma at a two-dimensional interface spanning the computational domain. Therefore, only the dynamics of the jet head and the propagation of a shock in the downstream region are studied. This simulation system is similar to simulations performed previously using effectively infinite counterstreaming jets. The important difference between this simulation and previous simulations is that the evolution of the Weibel instability is examined in a more realistic spatial way including motion of the jet head. Furthermore, the density of the jet relative to the ambient plasma can be changed easily. The Weibel instability is excited and the electron density is perturbed, as shown in Figure 2*a*. The electrons are deflected by the perturbed (small) transverse magnetic fields (B_x, B_y) via the Lorentz force: $-e(\boldsymbol{v}\times\boldsymbol{B})$, generating filamented current perturbations (J_z), which enhance the transverse magnetic fields (Weibel 1959; Medvedev & Loeb 1999). The complicated current structures due to the Weibel instability are shown in Figure 2*b*. The sizes of these structures are nearly the electron skin depth (4.8Δ). This is in good agreement with $\lambda \approx 2^{1/4} c\gamma_{\rm th}^{1/2}/\omega_{pe} \approx 1.188\lambda_{ce} = 5.7\Delta$ (Medvedev & Loeb 1999). Here $\gamma_{\rm th}$ is a thermal Lorentz factor and ω_{pe} is the electron plasma frequency. The shapes are elongated along the direction of the jet (the z-direction, horizontal in Fig. 2).

The acceleration of electrons has been reported in previous work (Silva et al. 2003; Frederiksen et al. 2003). As shown in Figure 3, the kinetic energy (parallel velocity $v_\parallel \approx v_j$) of the jet electrons is transferred to the perpendicular velocity via the electric and magnetic fields generated by

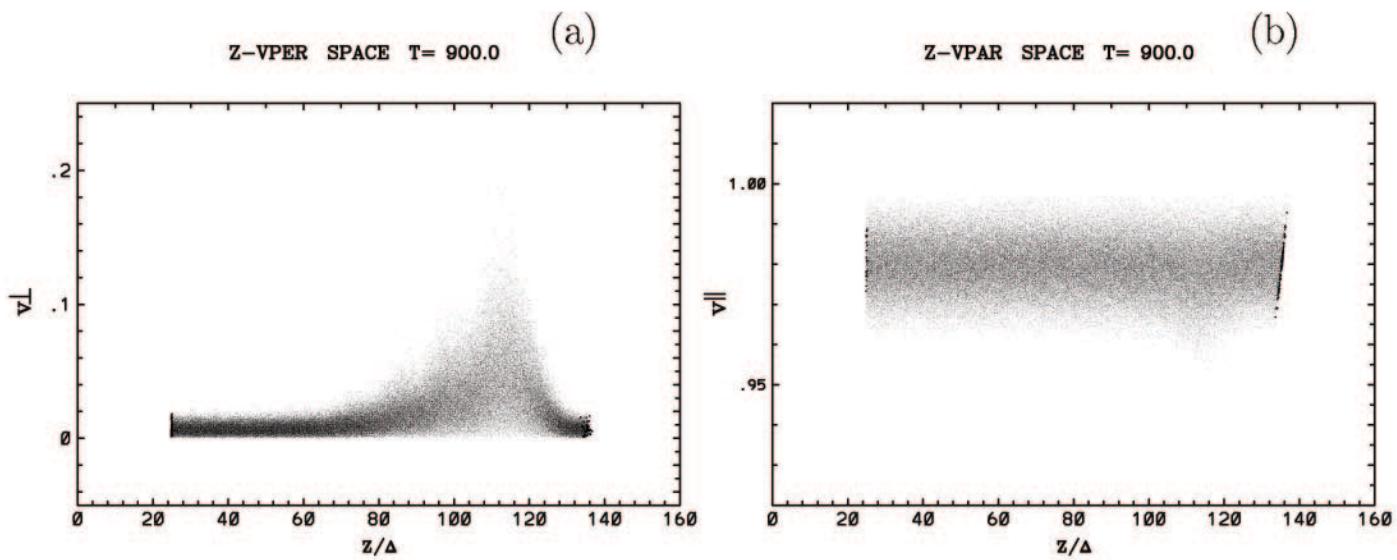

FIG. 3.—Distribution of jet electrons at $\omega_{pe}t = 23.4$ in (*a*) z-$v_\perp/c$ and (*b*) z-$v_\parallel/c$ phase space. Roughly 20% of the jet electrons are randomly selected for these plots. (*a*) Jet electrons are accelerated perpendicularly [$v_\perp = (v_x^2 + v_y^2)^{1/2}$] due to the nonuniform electric and magnetic fields. (*b*) Jet electrons are decelerated while they are accelerated perpendicularly around $z = 112\Delta$. The parallel velocity slanting at the jet head ($z = 136\Delta$) is due to the acceleration and deceleration and may be the result of Fermi acceleration.

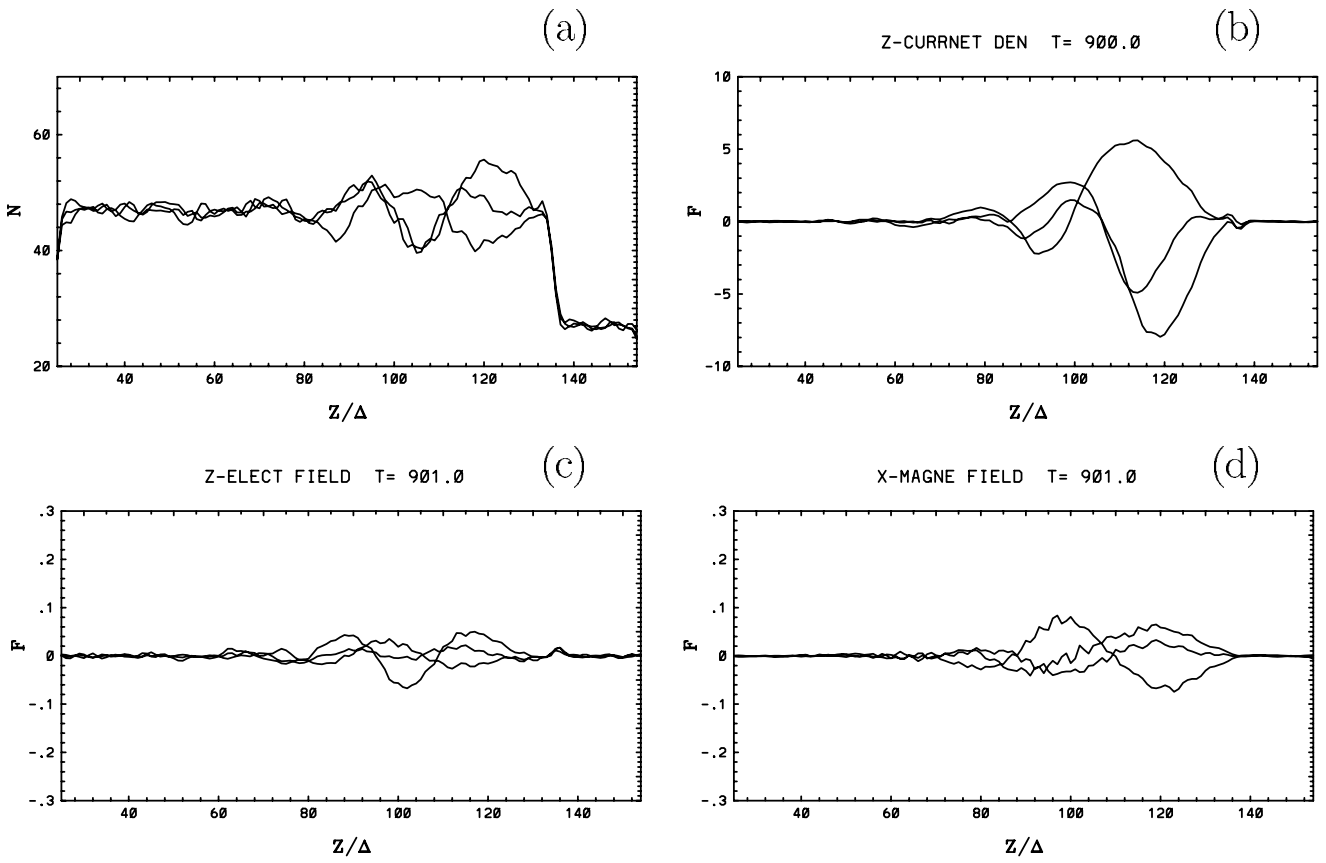

FIG. 4.—One-dimensional displays along the z-direction ($25 \leq z/\Delta \leq 154$) of (*a*) the electron density, (*b*) the z-component of the current density, (*c*) the z-component of the electric field, and (*d*) the x-component of the magnetic field at $\omega_{pe}t = 23.4$. The three curves are obtained at $x/\Delta = 38$ and $y/\Delta = 38, 43$, and 48. Due to the separation by the electron skin depth ($\lambda_{ce} \approx 4.8\Delta$), each curve shows the value at the different node of the growing Weibel instability.

the Weibel instability. The strongest deceleration of electron flow (Fig. 3*b*) and strongest transverse acceleration (Fig. 3*a*) is between $z/\Delta = 100$–120 and takes place around the maximum amplitude of perturbations due to the Weibel instability at $z = 112\Delta$ (see Figs. 2 and 4). On the other hand, jet ions are slightly accelerated (not shown). However, due to the larger mass of the ions, the energy gained by ion acceleration is similar to that gained by the electrons. Furthermore, at the jet front some jet electrons are accelerated and some are decelerated. This acceleration and deceleration is shown by the slanting in the parallel velocity distribution at the jet head (Fig. 3*b*). This may indicate that Fermi acceleration is taking place at the jet front as described in previous work (e.g., Achterberg et al. 2001; Gallant 2002; Ellison & Double 2002).

The Weibel instability is excited just behind the jet head as shown in Figure 4. The three curves are measured at three different locations ($y/\Delta = 38, 43$, and 48) about the electron skin depth apart. As a result the phase of instability is different, but the amplitudes are similar. The growth rate of the Weibel instability is calculated to be $\tau \approx \gamma_{\rm sh}^{1/2}/\omega_{pe} \approx 21.4$ ($\gamma_{\rm sh} = 5$) (Medvedev & Loeb 1999). This is in good agreement with the simulation results with the jet head located at $z = 136\Delta$. Figure 3 suggests that the "shock" has a thickness from about $z/\Delta = 80$–130 behind the shock front. Possibly, the "turbulence" assumed for the DSA corresponds to this shock region. The transverse acceleration of jet electrons takes place in the shock, as shown in Figure 3*a*. Subtle structures are recognized at the jet head ($z = 136\Delta$). As shown in Figure 4*a*, the width of the jet head is nearly the electron skin depth (4.8Δ). Additionally, Figure 4*b* shows that the z-component of current density becomes slightly negative. This results from the fact that some jet electrons are ahead of the ions. This negative current at $z = 137\Delta$ is clearly shown in Figure 5*b*. On the basis of Figures 2 and 4, the size of perturbations along the jet around $z = 120\Delta$ is nearly twice the electron skin depth. This result is consistent with the previous simulations by Silva et al. (2003).

The Weibel instability is excited just behind the jet head located at $z = 136\Delta$ (see Fig. 5*c*: $z = 134\Delta$), and the accelerated jet electrons are creating the negative current at $z = 137\Delta$ (Fig. 5*b*) just in front of the jet head. This total negative current is indicated by three curves dipped uniformly at $z = 137\Delta$ in Figure 4*b*.

The Weibel instability creates elongated shell-type structures which are also shown in counterstreaming jet simulations (Silva et al. 2003; Frederiksen et al. 2003). The size of these structures transverse to the jet propagation is nearly the electron skin depth (4.8Δ), as shown in Figures 5 and 6. It should be noted that the size of perturbations at $z = 120\Delta$ is larger than those at different locations, since the smaller scale perturbations merge to larger sizes in the nonlinear stage at the maximum amplitudes (Silva et al. 2003).

3.2. *Injection into Unmagnetized Ambient Plasma* (*Flat Jet*)

In the previous simulations of Silva et al. (2003) and Frederiksen et al. (2003) ambient magnetic fields are not

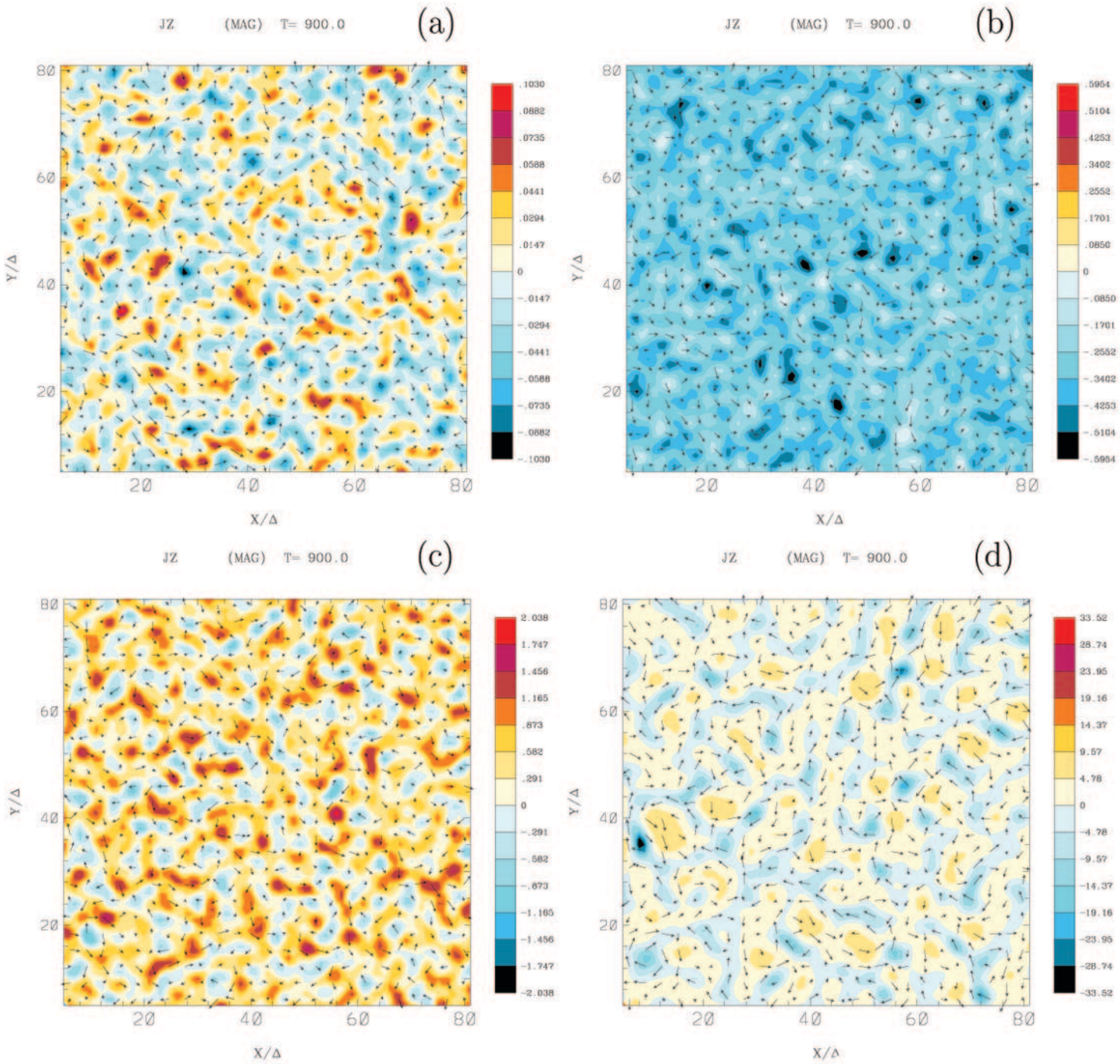

FIG. 5.—z-component of the current density in the x-y plane is plotted at z/Δ of (*a*) 140, (*b*) 137, (*c*) 134, and (*d*) 120. The maximum amplitudes of these panels are (*a*) 0.03 (thermal noise level), (*b*) 0.59, (*c*) 2.03, and (*d*) 7.0 (peak: 33.52), respectively. The sizes of current structures are larger at (*d*) $z = 120\Delta$, where the Weibel instability grows to the maximum amplitude (see Fig. 4), and smaller cells have nonlinearly merged into larger cells. [*See the electronic edition of the Journal for a color version of this figure.*]

included initially. In order to investigate the generation of magnetic fields, a simulation has been performed without ambient magnetic fields but otherwise with the same parameters.

The structure of perturbations to the electron density and z-component of the current density are similar to those with initial ambient magnetic fields (B_{0z}), as shown in Figure 7. The unmagnetized jet generates magnetic fields due to the current structures produced in the Weibel instability, as shown in Figures 7*b* and 8*b*. The peak values of the perturbations due to the Weibel instability for an unmagnetized ambient plasma is larger that those for a magnetized ambient plasma. However, the amplitude of these perturbations is similar; therefore the effects of initial ambient magnetic fields are not apparent in these cases. Further investigation is required for a systematic analysis of the effects of magnetic fields. The generation of magnetic fields both with and without an initial magnetic field suggests that synchrotron emission (or jitter radiation) is relevant in GRB afterglows and Crab-like pulsar winds (Medvedev 2000).

Figure 9 shows the structures of perturbations along the z-direction in electron density, J_z, E_z, and B_x, without an initial magnetic field. These are very similar to those with an initial magnetic field, shown in Figure 4. The three curves

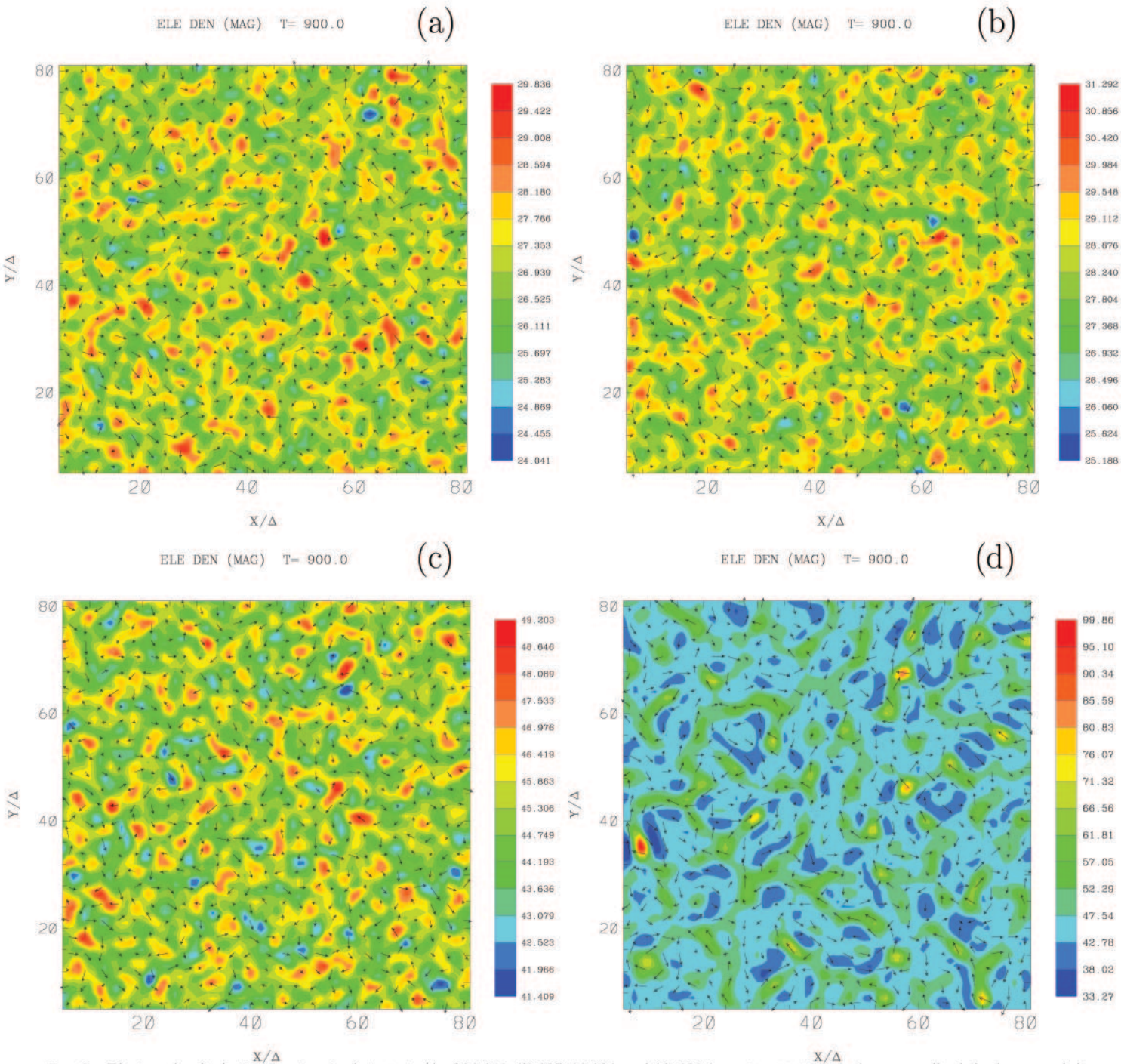

FIG. 6.—Electron density in the x-y plane is plotted at z/Δ of (*a*) 140, (*b*) 137, (*c*) 134, and (*d*) 120 (as in Fig. 5). The maximum amplitude in these panels is (*a*) 29.8 (the ambient plasma with thermal noise), (*b*) 31.2, (*c*) 49.2, and (*d*) 70 (peak: 99.8), respectively. The unperturbed average electron densities in the ambient and the total (jet plus ambient) plasma are 27 and 47, respectively. The size of the density perturbation structures is larger around $z/\Delta = 120$ (*d*), since the Weibel instability grows to the maximum amplitude (as shown in Fig. 4*a*) since smaller cells are merged nonlinearly into larger cells. The maximum density at $z/\Delta = 137$ (*b*) is 31.2; thus the jet head is located here, as indicated by Figs. 3*b* and 4*a*. [*See the electronic edition of the Journal for a color version of this figure.*]

are measured at three different locations ($y/\Delta = 38, 43$, and 48) each separated about 1 electron skin depth. The phase of the instability is different along each line, but the amplitudes are similar. Furthermore, the different seed perturbations (thermal noise by the initial loading of particles) and the unmagnetized plasma make the amplitudes and shape of perturbations at the nonlinear phase different from those with the magnetized plasma (as shown in Fig. 4). From the previous simulations without an initial ambient magnetic field (Silva et al. 2003; Frederiksen et al. 2003), highly nonuniform, small-scale magnetic fields are generated due to the Weibel instability.

4. SUMMARY AND DISCUSSIONS

We have performed the first self-consistent, three-dimensional relativistic particle simulations of electron-ion relativistic jets propagating through magnetized and unmagnetized electron-ion ambient plasmas. The Weibel instability is excited in the downstream region behind the jet

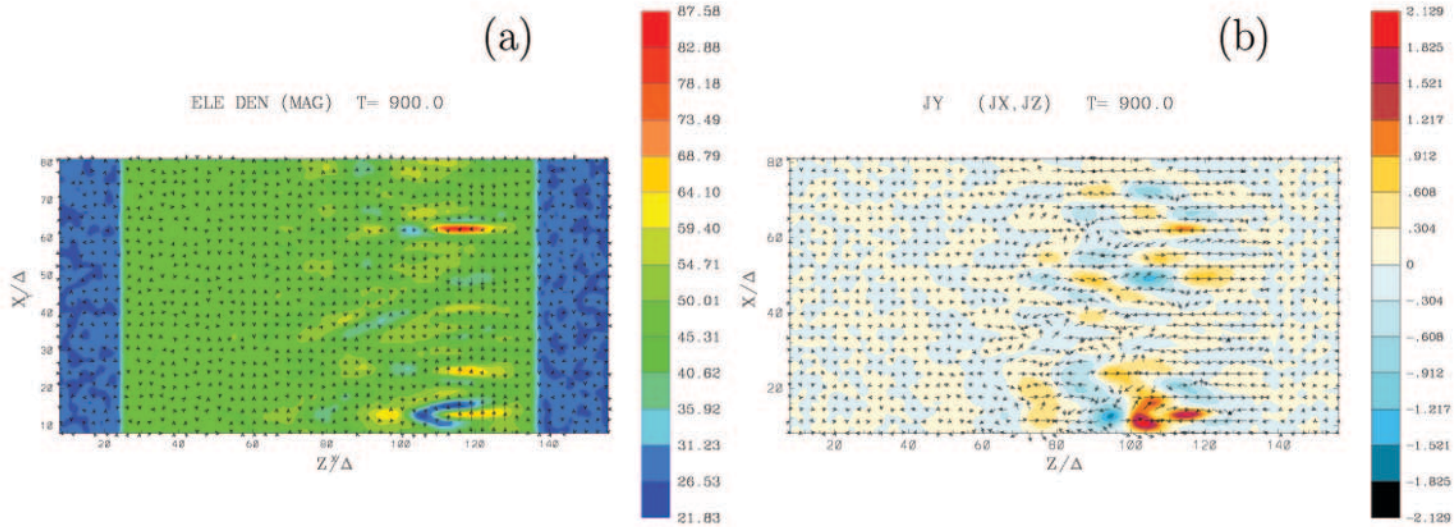

FIG. 7.—For the simulation with an unmagnetized ambient plasma, the Weibel instability is illustrated in two-dimensional images in the x-z plane in the center of the jet ($y = 43\Delta$ at $\omega_{pe}t = 23.4$). In (a) the colors indicate the electron density with magnetic fields represented by arrows and in (b) the colors indicate the y-component of the current density J_y, with J_z, J_x indicated by the arrows. The Weibel instability perturbs the electron density, leading to nonuniform currents and highly structured magnetic fields. These plates correspond to those in Fig. 2, but the color scales are different. The patterns are similar, however, the peak values with an unmagnetized ambient plasma are larger than those in the magnetized case.

head, where electron density perturbations and filamented currents are generated. The nonuniform electric field and magnetic field structures slightly decelerate the jet electrons and ions, while accelerating (heating) the jet electrons and ions in the transverse direction, in addition to accelerating the ambient material. The origin of the Weibel instability relies on the fact that the electrons are deflected by the perturbed (small) transverse magnetic fields (B_x, B_y), and subsequently enhance the filamented current (Weibel 1959; Medvedev & Loeb 1999; Brainerd 2000; Gruzinov 2001). The deflection of particle orbits due to the Lorentz force increases as the magnetic field perturbation grows in amplitude. The amplified magnetic field is random in the direction perpendicular to the particle motion, since it is generated from a random seed field. The perturbed electron density and filamented currents have a complicated three-dimensional structure. The transverse size of these structures is nearly equal to the electron skin depth but is larger if there are no ambient magnetic fields. However, the size along the direction of jets is larger than the transverse scales. At the termination of our simulation, the thickness of the unstable region along the jet direction ranges from

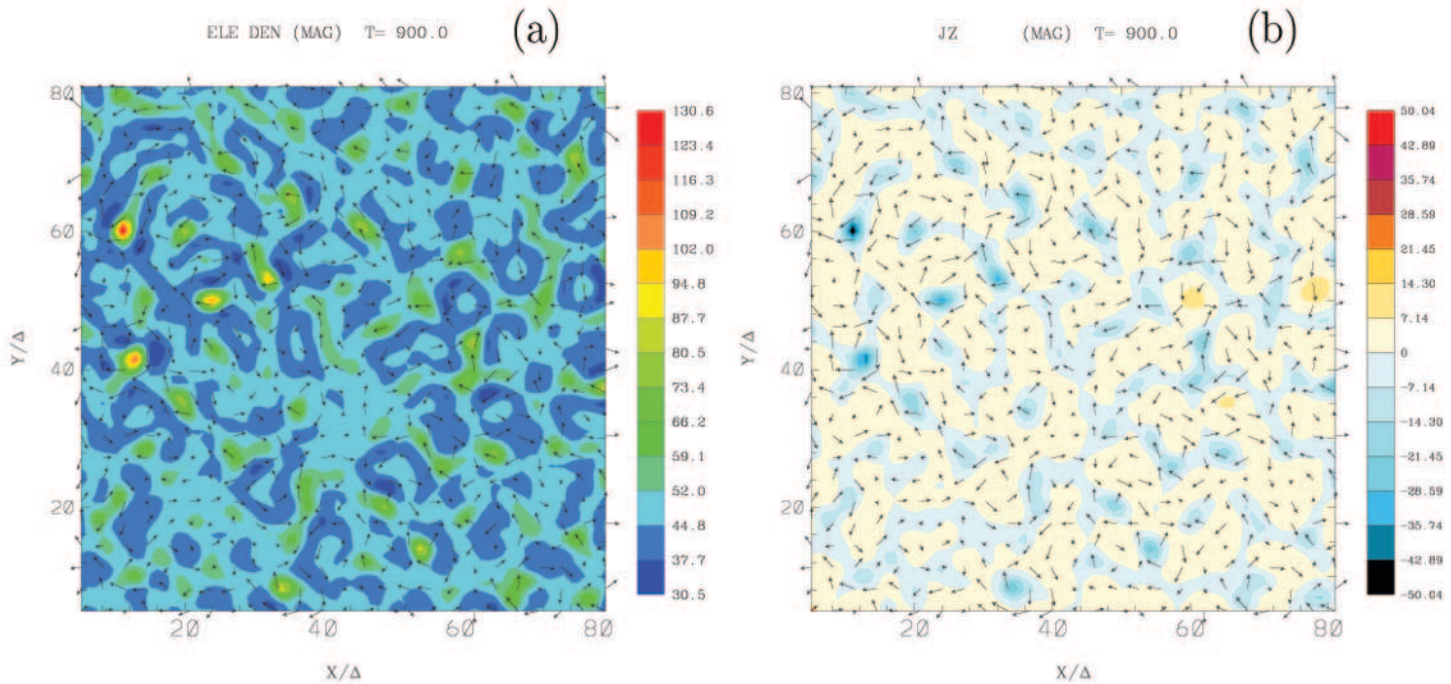

FIG. 8.—(a) Electron density and (b) z-component of the current density are plotted in the x-y plane at $z = 120\Delta$. The maximum amplitudes of these panels are (a) 70 (peak: 130; compare to Fig. 6d) and (b) 10 (peak: 50; compare to Fig. 5d). The size of the current structures is similar to those found with an ambient magnetic field. These plates correspond to Figs. 6d and 5d, respectively. [*See the electronic edition of the Journal for a color version of this figure.*]

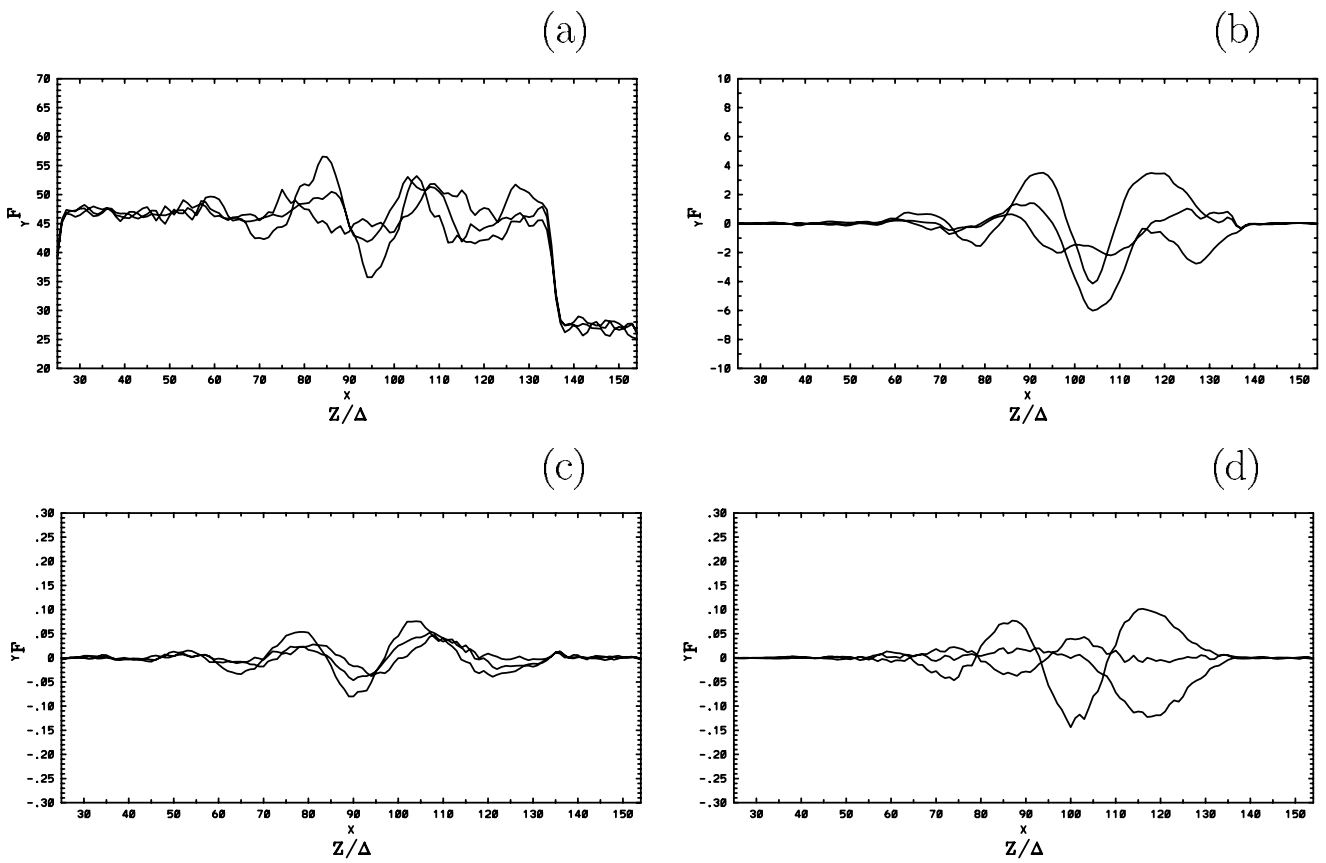

FIG. 9.—One-dimensional displays along (*a*) the *z*-direction of the electron density, (*b*) the *z*-component of the current density, (*c*) the *z*-component of the electric field, and (*d*) the *x*-component of the magnetic field at $\omega_{pe}t = 23.4$. The three curves are obtained at $x/\Delta = 38$ and $y/\Delta = 38, 43$, and 48. These plates correspond to those in Fig. 4. [*See the electronic edition of the Journal for a color version of this figure*.]

$z/\Delta = 80$ to 130. The perturbation size in the transverse direction become largest around $z/\Delta = 120$, where nonlinear effects lead to the merging of the smaller scale filaments that first appear behind the jet front. This result is similar to previous counterstreaming simulation results (Silva et al. 2003) in which smaller scale filaments first appear and then merge into larger scale filaments at a later time. Now we see the temporal development appear as a spatial development.

The simulation results show that the initial jet kinetic energy goes to the magnetic fields and transverse acceleration of the jet particles through the Weibel instability. The properties of the synchrotron or "jitter" emission from relativistic shocks are determined by the magnetic field strength, $\boldsymbol{B}$, and the electron energy distribution behind the shock. The following dimensionless parameters are used to estimate these values: $\epsilon_b = U_b/e_{\rm th}$ and $\epsilon_e = U_e/e_{\rm th}$ (Medvedev & Loeb 1999). Here $U_b = B^2/8\pi$ and U_e are the magnetic and electron energy densities, and $e_{\rm th} = nm_ic^2(\gamma_{\rm th} - 1)$ is the total thermal energy density behind the shock, where m_i is the ion mass, n is the ion number density, and $\gamma_{\rm th}$ is the mean thermal Lorentz factor of ions. On the basis of the available diagnostics, the following values are estimated: $\epsilon_b \approx 0.02$ and $\epsilon_e \approx 0.3$ (typical values for GRB afterglows). These estimates are made at the maximum amplitude ($z \approx 112\Delta$).

The basic nature of the Weibel instability is as follows (Medvedev & Loeb 1999):

1. The instability is aperiodic; i.e., $\omega_{\rm real} = 0$ (convective). Thus, it can be saturated only by nonlinear effects and not by kinetic effects, such as collisionless damping or resonance broadening. Hence the magnetic field can be amplified to very high values.

2. The instability is self-saturating. It continues until all the free energy due to the particle distribution function anisotropy is transferred to the magnetic field energy.

3. The produced magnetic field is randomly oriented in the direction perpendicular to the flow. The Lorentz forces randomize particle motion over the pitch angle and hence introduce an effective scattering into the otherwise collisionless system.

To this basic nature we add the spatial development associated with the propagation of the jet front:

1′. The smaller scale filaments appear immediately behind the jet front. The nonlinear effect is recognized by the fact that smaller filaments merge into larger filaments behind the jet front, as shown in Figures 5 and 6.

2′. The instability is self-saturating (spatially) behind the jet front and continues until all of the free energy due to the particle distribution function anisotropy is transferred to the magnetic field energy. The largest amplitude of perturbations is located near the region with the maximum transverse acceleration (Fig. 3*a*) with deceleration in parallel velocity (v_z) (Fig. 3*b*), as shown in Figures 2, 5*d*, and 6*d*.

3′. The produced magnetic field is randomly oriented in the "shock" plane (three-dimensional structure, as shown in Figs. 2*b* and 5). The random Lorentz forces result in randomization and deceleration of the jet particles, an

acceleration of the ambient particles, and transverse acceleration (heating) of jet and ambient particles inside the "shock" region.

Previous microphysical analyses of the energy conversion in relativistic pair outflows interacting with the surrounding interstellar medium consisting of cold protons and electrons have been performed (e.g., Brainerd 2000; Schlickeiser et al. 2002). These analyses have demonstrated that the beam excites both electrostatic and low-frequency magnetohydrodynamic Alfvén-type waves via a two-stream instability in the background plasma. They have also provided the time evolution of the distribution functions of beam particles and the generated plasma wave turbulence power spectra. While the jet front showed evidence of Fermi acceleration, the main acceleration of electrons may take place in the downstream region (e.g., Brainerd 2000; Schlickeiser et al. 2002; Ostrowski & Bednarz 2002).

Our present simulation study has provided the framework of the fundamental dynamics of a relativistic shock generated within a relativistic jet. While some Fermi acceleration may occur at the jet front, the majority of electron acceleration takes place behind the jet front and cannot be characterized as Fermi acceleration. Since the shock dynamics is complex and subtle, further comprehensive study is required for better understanding of the acceleration of electrons and the associated emission as compared with current theory (e.g., Rossi & Rees 2003). This further study will provide more insight into basic relativistic collisionless shock characteristics. The fundamental characteristics of such shocks are essential for a proper understanding of the prompt gamma-ray and afterglow emission in gamma-ray bursts and also to an understanding of the particle reacceleration processes and emission from the shocked regions in relativistic AGN jets.

K. N. is a NRC Senior Research Fellow at NASA Marshall Space Flight Center. This research (K. N.) is partially supported by NSF ATM-9730230, ATM-9870072, ATM-0100997, and INT-9981508. The simulations have been performed on ORIGIN 2000 and IBM p690 (Copper) at the National Center for Supercomputing Applications, which is supported by NSF.

REFERENCES

Achterberg, A., Gallant, Y. A., Kirk, J. G., & Guthmann, A. X. 2001, MNRAS, 328, 393
Birdsall, C. K., & Langdon, A. B. 1995, Plasma Physics via Computer Simulation (2d ed.; New York: McGraw-Hill)
Brainerd, J. J. 2000, ApJ, 538, 628
Buneman, O. 1993, in Computer Space Plasma Physics: Simulation Techniques and Software, ed. H. Matsumoto & Y. Omura (Tokyo: Terra Scientific Publ. Co.), 67
Dawson, J. M. 1983, Rev. Mod. Phys., 55, 403
Ellison, D. C., & Double, G. P. 2002, Astropart. Phys., 18, 213
Frederiksen, J. T., Hededal, C. B., Haugbølle, & Nordlund, Å. 2003, Proc. 1st NBSI on Beams and Jets in Gamma Ray Bursts, NBIfAFG/NORDITA, Copenhagen, 2002 August (astro-ph/0303360)
Gallant, Y. A. 2002, in Particle Acceleration at Relativistic Shocks, in Relativistic Flows in Astrophysics, ed. A. W. Guthmann, M. Georganopoulos, A. Marcowith, & K. Manolokou (Lecture Notes in Physics 589; Berlin: Springer), 24
Gruzinov, A. 2001, ApJ, 563, L15
Hockney, R. W., & Eastwood, J. W. 1988, Computer Simulation using Particles (2d ed.; New York: McGraw-Hill)
Medvedev, M. V. 2000, ApJ, 540, 704
Medvedev, M. V., & Loeb, A. 1999, ApJ, 526, 697
Nishikawa, K.-I., Zhao, J., Sakai, J. I., & Neubert, T. 1997, Adv. Space. Res., 19, (1)117
Ostrowski, M., & Bednarz, J. 2002, A&A, 394, 1141
Pruet, J., Abazajian, K., & Fuller, G. M. 2001, Phys. Rev. D., 64, 063002-1
Rossi, E. & Rees, M. J. 2003, MNRAS, 339, 881
Schlickeiser, R., Vainio, R., Böttcher, M., Lerche, I., Pohl, M., & Schuster, C. 2002, A&A, 393, 69
Silva, L. O., Fonseca, R. A., Tonge, J. W., Dawson, J. M., Mori, W. B., & Medvedev, M. V. 2003, ApJL, submitted
Weibel, E. S. 1959, Phys. Rev. Lett., 2, 83
Zhao, J., Sakai, J. I., Nishikawa, K.-I., & Neubert, T. 1994, Phys. Plasmas, 1, 4114